CNF1 Exploits the Ubiquitin-Proteasome Machinery to Restrict Rho GTPase Activation for Bacterial Host Cell Invasion

Anne Doye,[1] Amel Mettouchi,[3] Guillaume Bossis,[4]
René Clément,[1] Caroline Buisson-Touati,[1]
Gilles Flatau,[1] Laurent Gagnoux,[2]
Marc Piechaczyk,[4] Patrice Boquet,[1]
and Emmanuel Lemichez[1,5]
[1]INSERM U452, IFR 50
[2]INSERM U385, IFR 50
Faculté de Médecine
28 avenue de Valombrose
06107 Nice
France
[3]CNRS-UMR 6543, IFR 72
Centre Antoine Lacassagne
33 avenue de Valombrose
06189 Nice
France
[4]CNRS-UMR 5535, IFR 24
Institut de Génétique Moléculaire
1919 route de Mende
34293 Montpellier
France

Summary

CNF1 toxin is a virulence factor produced by uropathogenic *Escherichia coli*. Upon cell binding and introduction into the cytosol, CNF1 deamidates glutamine 63 of RhoA (or 61 of Rac and Cdc42), rendering constitutively active these GTPases. Unexpectedly, we measured in bladder cells a transient CNF1-induced activation of Rho GTPases, maximal for Rac. Deactivation of Rac correlated with the increased susceptibility of its deamidated form to ubiquitin/proteasome-mediated degradation. Sensitivity to ubiquitylation could be generalized to other permanent-activated forms of Rac and to its sustained activation by Dbl. Degradation of the toxin-activated Rac allowed both host cell motility and efficient cell invasion by uropathogenic bacteria. CNF1 toxicity thus results from a restricted activation of Rho GTPases through hijacking the host cell proteasomal machinery.

Introduction

The CNF1 toxin is a virulence factor produced by uropathogenic *Escherichia coli* (UPEC) strains, responsible for urinary tract infections (Blanco et al., 1992; Landraud et al., 2000). CNF1 is also associated with other extraintestinal pathogenic *E. coli* such as those of serotype K1 implicated in neonatal meningitis (Bonacorsi et al., 2000; Khan et al., 2002). More recently, a CNF1-like toxin has been found in *Yersinia pseudotuberculosis* (Lockman et al., 2002).

Currently, CNF1 is the paradigm of the Rho GTPase-activating bacterial toxins (Boquet, 2001). The amino-terminal part of the toxin contains the receptor binding

[5]Correspondence: lemichez@hermes.unice.fr

domain (Lemichez et al., 1997). The enzymatic domain, localized at the carboxy-terminal end, is translocated into the cytosol, where it activates Rho GTPases (Pei et al., 2001). CNF1 catalyzes a deamidation reaction, which specifically modifies glutamine 63 of RhoA or its equivalent (glutamine 61) in Rac and Cdc42 into glutamic acid, conferring on Rho GTPases the properties of dominant-positive mutants by inactivation of their intrinsic and GAP-regulated capacity for GTP hydrolysis (Flatau et al., 1997; Schmidt et al., 1997; Lerm et al., 1999a). The specificity of CNF1-induced Rho GTPase modification is conferred, on the toxin side, by a deep cavity in which the critical deamidase catalytic residues are located (Buetow et al., 2001). CNF1 target specificity is determined by a short amino acid sequence encompassing glutamine 61/63 of the switch 2 domain, which is highly conserved in Rho, Rac, and Cdc42 (Lerm et al., 1999b; Flatau et al., 2000).

Rho small GTPases were first characterized as regulators of the actin cytoskeleton (Chardin et al., 1989; Paterson et al., 1990; Hall, 1998). Their signaling activities have since been extended to a large variety of cellular processes, including the crosstalk between bacteria and their hosts. Consistent with this, an increasing number of microbial virulence factors and toxins have been found to interfere with Rho GTPases (Boquet et al., 1998; Stebbins and Galán, 2001). Most bacterial toxins target Rho GTPases to induce their inactivation. Surprisingly, CNF1 and the related dermonecrotic toxin (DNT) from *Bordetella* have opposite effects (Boquet, 2001; Horiguchi, 2001). The gain of function conferred by CNF1 to Rho GTPases remains therefore to be elucidated.

In the present study, we have investigated the extent of Rho GTPase activation by the uropathogenic *E. coli* CNF1 toxin in the context of bladder epithelial cells. This allowed us to demonstrate that CNF1 exploits the ubiquitin-proteasome machinery to confer invasive properties to uropathogenic *E. coli*.

Results

CNF1 Induces a Transient Activation of Rho GTPases

Owing to the relationship established between CNF1- and UPEC-borne infections, we investigated the in vivo effects of the toxin using the 804G-rat bladder carcinoma cell line. The use of activated Rho GTPase pull-down assays enabled us to quantify the levels of CNF1-induced Rho GTPase activation, although it did not allow us to differentiate between wild-type and deamidated active forms of Rho (Manser et al., 1998; Ren et al., 1999). Nevertheless, pull-down assays offered us an approach to investigate the relationships between the cellular effects of CNF1 and the level of activation of each Rho GTPase. Cells were treated with CNF1 and subjected to pull-down assays after different periods of time (Figure 1A). These experiments revealed two new findings. We observed that CNF1 induced a transient activation of Rac, RhoA, and Cdc42, instead of their
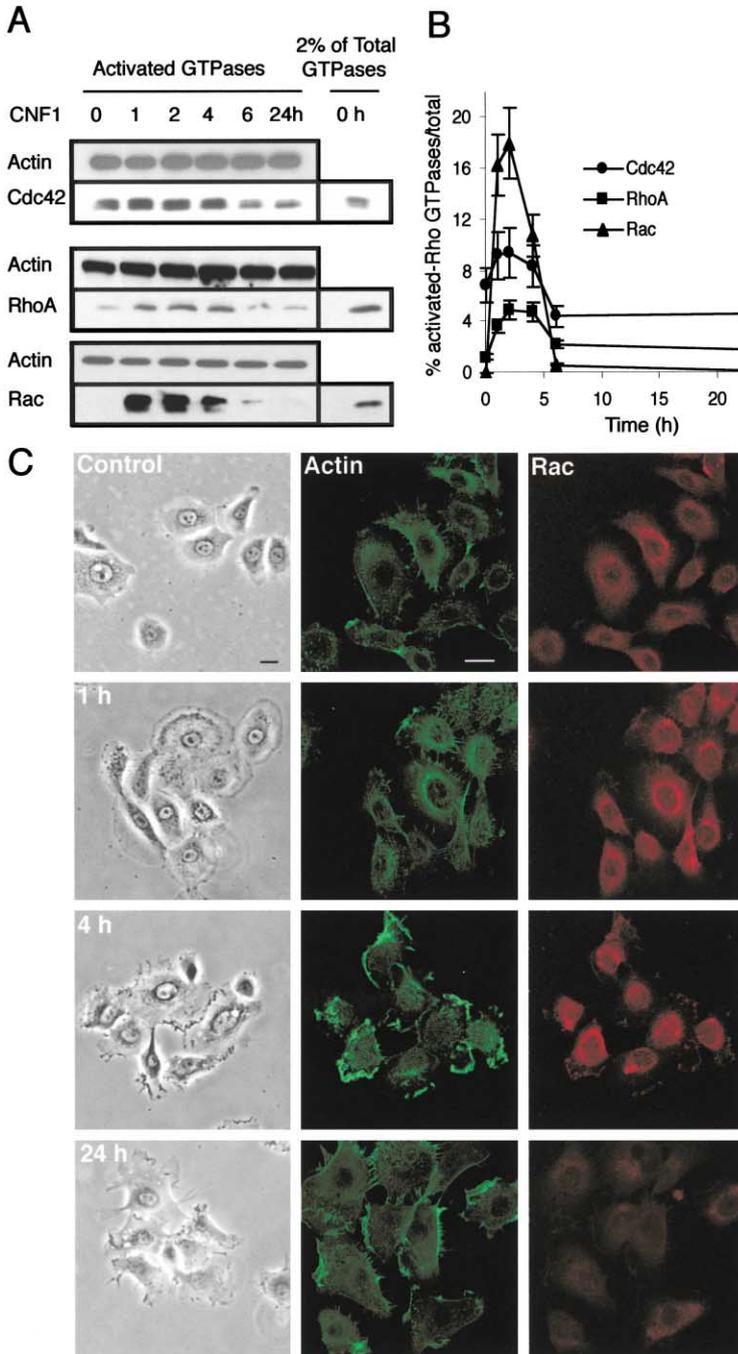
A

B

C

Figure 1. CNF1 Induces a Transient Activation of Rho GTPases

(A) Immunoblots showing the kinetics of CNF1-induced activation of Rho GTPases in 804G cells. Cells were treated with 10^{-9} M CNF1 for different periods of time. Cell lysates were subjected to the GST-fusion protein pull-down assays. Activated Rho GTPases bound to the GST-fusion proteins were resolved on SDS-PAGE and transferred on nylon membranes for immunoblotting. Two percent of the total CNF1-untreated lysate was loaded on the same gel to estimate the amount of cellular Rho GTPases engaged in the assay. In parallel, 10 μg of each cell lysate were processed for actin immunoblotting to verify protein amounts.

(B) Quantification of activated Rho GTPases. Immunoblots were scanned and quantified using NIH Image 1.6. The level of activated Rho GTPases was compared to the total Rho GTPase level present in 2% of the control cell lysate (CNF1-untreated) (mean value of three independent experiments ± SD).

(C) 804G cells were treated with 10^{-9} M CNF1 for different periods of time. Cells were processed for Rac immunolocalization together with actin cytoskeleton labeling, as described in the Experimental Procedures. From left to right, the first column corresponds to the light transmission pictures showing the effect of CNF1 on cell morphology. The second and third columns show the actin cytoskeleton and the Rac immunosignal, respectively. The bars equal 10 μm.

expected permanent activation. Rac activation appeared more transient as compared to that of RhoA and Cdc42. We also observed that CNF1 induced a maximal level of activated-Rac and Cdc42, in contrast to RhoA (Figure 1B). We further analyzed the effects of CNF1 on the actin cytoskeleton and cell morphology. We took advantage of the ability of Rho GTPases to be recruited on cellular endomembranes upon activation to investigate, by immunofluorescence, the behavior of Rac, which antibody gives a strong immunosignal in contrast to that from RhoA and Cdc42. Intoxicated cells were analyzed at different time periods, according to the pull-down measurements, to visualize the localization of activated and downregulated forms of Rac (Figure 1C). Filamentous actin was labeled together with Rac. Immunofluorescence signals were analyzed, using confocal microscopy conditions, which allowed us to compare signal intensities. The 804G control cells displayed mostly filopodia at their periphery. In such conditions, the Rac immunosignal appeared cytosolic together with a fraction associated with endomembranes forming perinuclear vesicles. After 1 hr of intoxication with CNF1, cells displayed a strong spreading, as visualized by light transmission microscopy. Spreading was followed by cell retraction after 4 hr of CNF1 treatment. During the first 4 hr of CNF1 treatment, cells displayed a higher

A

B

C

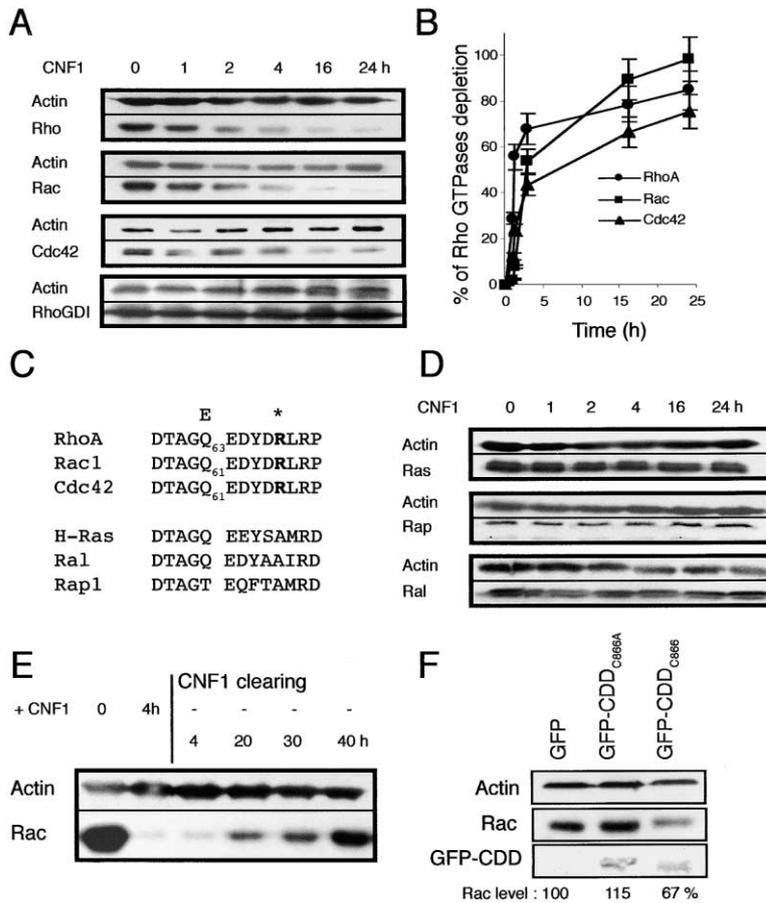|	E	*
RhoA	DTAGQ$_{63}$EDYDRLRP	
Rac1	DTAGQ$_{61}$EDYDRLRP	
Cdc42	DTAGQ$_{61}$EDYDRLRP	
H-Ras	DTAGQ EEYSAMRD	
Ral	DTAGQ EDYAAIRD	
Rap1	DTAGT EQFTAMRD	

D

E

F

Rac level : 100   115   67 %

Figure 2. Kinetics and Specificity of CNF1-Induced Rho GTPase Depletion

(A) Immunoblots showing the kinetics of CNF1-induced Rho GTPases depletion. 804G cells were treated for different times with 10^{-9} M CNF1. Cells were lysed in Laemmli buffer and immunoblots performed using 30 μg of total protein lysate. Immunoblots anti-actin were used to verify equal loading and normalize Rho GTPase signals.

(B) Quantification of the CNF1-induced Rho GTPase depletion (mean value of two independent experiments ± SD).

(C) Sequences of the Ras-related proteins studied for CNF1 sensitivity were aligned in the region surrounding the CNF1-deamidated glutamine 61 of Rac1 and Cdc42 or 63 of RhoA. Asterisk indicates RhoA arginine 68, which confers the specificity of Rho GTPase recognition by CNF1.

(D) Immunoblots showing the stability of other Ras-related GTPases during CNF1 intoxication. Cell intoxication and immunoblots were performed as described above.

(E) CNF1-induced Rac depletion is reverted upon toxin clearing. After 4 hr of intoxication with 10^{-9} M CNF1, 804G cells were extensively washed in PBS and further incubated in toxin-free medium. Cells were processed at different times for Rac immunoblotting as described above.

(F) Effect of the expression of CNF1 deamidase domain on Rac-induced cell depletion. 804G cells were transfected with either GFP or GFP-CDD$_{C866}$ (wild-type deamidase domain) or GFP-CDD$_{C866A}$ (inactivated deamidase domain). After 6 hr of transgene expression, Rac depletion was estimated by immunoblotting, and equal expression of GFP-CDD constructs was verified by anti-GFP immunoblotting.

content of filamentous actin. In parallel, we observed a partial relocalization of Rac from the cytosol to the plasma membrane and perinuclear vesicles. Most remarkably, after 24 hr of continuous intoxication by CNF1, cells exhibited a dramatic decrease of Rac immunosignal. These results suggested that the transient activation of Rac induced by the toxin might have resulted from a cellular depletion of this GTPase. Transient recruitment of Rho GTPases to cellular membranes was confirmed by cellular fractionation (not shown).

CNF1 Induces the Specific Depletion of Rho GTPases

The cellular content of Rho GTPases was analyzed by immunoblotting (Figure 2A). The loss of Rho GTPases was almost complete after 24 hr of CNF1 treatment (Figure 2A). The decrease was more dramatic for Rac, as compared to RhoA and Cdc42 (Figure 2B). The initial speed of clearance, measured between 30 and 90 min after intoxication, was maximal for RhoA ($a_{RhoA} = 0.50\%$/min) when compared to that of Cdc42 and Rac ($a_{Cdc42} = 0.21\%$/min and $a_{Rac} = 0.15\%$/min, respectively). Notably, the Rho GDP-dissociating inhibitor (RhoGDI) protein level remained stable during CNF1 intoxication (Figure 2A). To investigate whether CNF1-induced Rho GTPase depletion was restricted to this particular Ras GTPase

subfamily, we investigated the stability of other small GTPases. In this respect, Ras, Ral, and Rap, which do not contain the specific amino acid sequence necessary to CNF1-mediated deamidation, were controlled for their toxin-induced cell depletion (Figure 2C; Lerm et al., 1999b; Flatau et al., 2000). In contrast to Rho GTPases, Ras, Ral, and Rap remained stable during CNF1 treatment (Figure 2D).

Considering that Rac exhibited the most transient and pronounced activation after cell intoxication, we focused on this small G protein in the following experiments. When CNF1 was provided to cells for 4 hr and then removed, we observed that the Rac immunosignal reappeared, indicating that the CNF1-induced depletion of Rac was a reversible process (Figure 2E). This latter finding, together with our observation showing the stability of Ras, Ral, and Rap, suggested that Rac depletion was not the result of a nonspecific CNF1-induced toxicity, but rather a consequence of the toxin-induced Rho GTPase modification. This led us to examine whether the CNF1 deamidase activity on Rac glutamine 61 might be specifically required to induce the GTPase depletion. We addressed this question by expressing in cells the minimum carboxy-terminal deamidating domain of the toxin (CDD), nonmodified or mutated in its catalytic cysteine 866 (Buetow et al., 2001). GFP-fusion proteins cor-
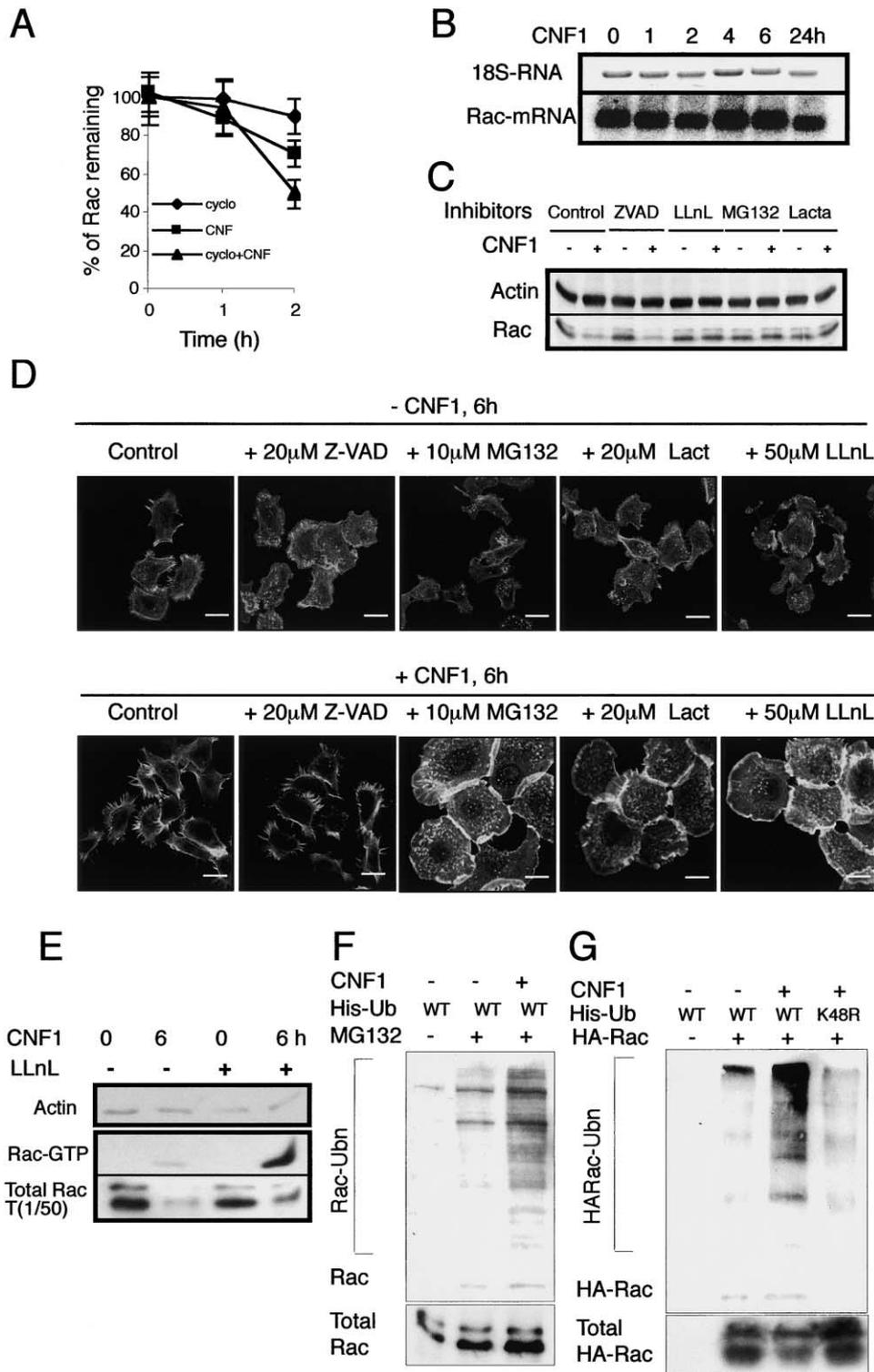
Figure 3. CNF1-Induced Rac Ubiquitylation and Proteasomal Degradation

(A) Comparison of Rac half-life in the presence or absence of CNF1, in 804G cells. Cells were pretreated 10 min with 10 μg·ml^{-1} cycloheximide (cyclo) followed by intoxication with 10^{-9} M CNF1 in the presence (cyclo+CNF) or absence of cycloheximide (CNF). The protein synthesis blocking effect of cycloheximide was verified by incorporation of L-[U-^{14}C]leucine (not shown). Cells were lysed in Laemmli buffer and endogenous Rac signal was quantified by immunoblot, normalized to actin immunosignal (mean value of three independent experiments ± SD).

(B) Stability of Rac mRNA during CNF1 intoxication of 804G cells. Northern blotting was performed using pXJ-Rac as a probe. Total RNA loading was visualized by 18S ribosomal RNA ethidium bromide staining.

(C) Immunoblots anti-Rac showing the blocking effects of proteasome inhibitors on the CNF1-induced Rac depletion. 804G cells were pretreated

responding to the CDD wild-type (GFP-CDD$_{C866}$) or mutated (GFP-CDD$_{C866A}$) were expressed in 804G cells. A 30% depletion of Rac was found only in the GFP-CDD$_{C866}$-expressing cells, a percentage similar to the transfection efficiency (Figure 2F). This indicated that the deamidase activity of CNF1 was required and sufficient to mediate Rac depletion.

**CNF1 Induces Rac Ubiquitylation
and Proteasome-Dependent Depletion**
The fact that CNF1 induced a posttranslational modification restricted to Rho GTPases led us to investigate the possible involvement of a degradative mechanism for the toxin-induced Rac depletion. In contrast to control cells, in which Rac appeared to be a stable protein (Figure 3A), we observed a decrease of Rac stability in CNF1-treated cells (half-life 115 min). The fact that both Rac stability and CNF1-induced Rac depletion half-lives were found to match closely ruled out a possible inhibition of Rac translation induced by the toxin (Figure 3A). That CNF1 did not affect the Rac mRNA levels was also verified (Figure 3B). Determination of the degradative machinery responsible for Rac depletion was investigated first using different cell-permeant protease inhibitors. Z-VAD, a blocker of caspase proteases, and three different proteasome/calpain protease inhibitors, among which lactacystin is the most specific for the proteasome, were tested. At the concentrations used, only proteasome inhibitors conferred a significant protection against CNF1-induced Rac depletion (Figure 3C). To rule out a possible inhibition of the CNF1-induced Rho GTPase deamidation/activation by proteasome inhibitors, we monitored the effects of CNF1 on the actin cytoskeleton and cell morphology (Figure 3D). The treatment of cells with CNF1 for 6 hr induced the formation of filopodia (Figures 3D and 1C). Furthermore, cells did not exhibit a higher content of F actin when compared to a control preparation. In contrast, upon addition of proteasome inhibitors during the CNF1 treatment, cells displayed a strong spreading together with an increased content of filamentous actin (Figure 3D). This indicated that proteasome inhibitors interfered with, rather than inhibited, the CNF1 effects on the cell cytoskeleton. We next tested the possibility that proteasome inhibitors might in fact increase the level of activated Rac upon CNF1 treatment. We observed that the level of activated

Rac in CNF1-treated cells was increased upon cotreatment with LLnL proteasome inhibitor (Figure 3E). This indicated that proteasome inhibitors were most probably acting by blocking the degradation of the pool of activated Rac. We therefore concluded that the proteasome machinery might be involved in the CNF1-induced clearance of Rac. Many short-living proteins are tagged by addition of an ubiquitin chain directing their specific degradation by the proteasome (Hershko and Ciechanover, 1998). To investigate the possibility of a CNF1-induced Rac ubiquitylation, we compared the amount of endogenous ubiquitylated Rac under different conditions. Histidine-tagged ubiquitin-transfected cells were treated either with MG132 alone or together with CNF1. We observed that treatment of cells with CNF1 induced a 2.3-fold greater appearance of Rac ubiquitylated forms (Rac-Ubn), as compared to control cells (Figure 3F). In addition, we observed a reduction of the ubiquitylated level of cotransfected HA-Rac using the ubiquitin mutant K48R, known to impair ubiquitin chain formation for proteasome targeting (Figure 3G; Chau et al., 1989). We have therefore established that CNF1 elicited an increase of Rac ubiquitylation, likely responsible for its CNF1-induced proteasome degradation.

**Ubiquitin Modification of Rac Results from Its
Sustained Activation**
Our results raised the question of whether CNF1-induced degradation of Rac was a consequence of its sole mutation or was due to its permanent activation. To discriminate between these possibilities, the steady-state levels of three permanently activated Rac mutants (Rac-Q61L, Rac-Q61E, and Rac-G12V) were compared to that of dominant-inactive Rac-T17N and Rac wild-type. Cells were transfected with both Rac mutants and GFP expression plasmids to normalize the amounts of proteins expressed. We observed that all three activated mutants were less stable than the wild-type and dominant-negative Rac proteins (Figure 4A). To investigate whether the instability of the Rac dominant-positive mutants depended on the proteasomal machinery, we compared their ubiquitylation sensitivity. Rac-Q61E exhibited a 3-fold higher sensitivity to ubiquitylation than the wild-type Rac, in accordance with the 2.3-fold induction of endogenous-Rac ubiquitylation measured in CNF1-intoxicated cells (Figures 4B and 3F). In addition, all

with the different protease inhibitors (20 μM Z-VAD, 50 μM LLnL, 10 μM MG132, and 20 μM Lactacystin) for 30 min before addition of 10^{-9} M CNF1. Upon 3 hr of CNF1 intoxication, cells were lysed in Laemmli buffer and processed for anti-Rac immunoblotting using 20 μg of total proteins. Cells treated with the drugs alone did not show changes in their total Rac content.
(D) FITC-phalloidin labeling of the actin cytoskeleton showing CNF1 effects on cell spreading and actin bundling in the presence of proteasome inhibitors. After 6 hr of 804G cells treatment with or without 10^{-9} M CNF1, in the presence or absence of protease inhibitors, the cells were labeled with FITC-phalloidin to visualize the actin cytoskeleton (the bars equal 10 μm).
(E) Addition of 50 μM LLnL proteasome inhibitor reinforces the CNF1-induced activation of Rac. After 6 hr of treatment, cells were processed for Rac GST-PAK[70-106] pull-down assay. The amount of proteins engaged in the pull-down assay was verified by actin immunoblotting (top).
(F) CNF1 intoxication of 804G cells results in an increase of Rac ubiquitylation. Cells expressing Histidine-tagged ubiquitin (His-Ub) were treated with 10 μM MG132 with or without 10^{-8} M CNF1 for 4 hr and processed for histidine-tagged ubiquitin purification (10^7 transfected cells for each condition). His-Ub crosslinked forms of endogenous Rac (noted Rac-Ubn) were visualized by immunoblotting anti-Rac. An anti-Rac immunoblot was performed in parallel on 1% of the total lysates to compare the amounts of total Rac engaged in the His-Ub purifications (bottom).
(G) 804G cells expressing HA-tagged wild-type Rac and/or Histidine-tagged ubiquitin wild-type (His-Ub WT) or K48R mutant (His-Ub K48R) were treated 15 hr with 10^{-8} M CNF1 and processed for histidine-tagged ubiquitin purification. His-Ub crosslinked forms of HA-Rac were visualized by immunoblotting anti-HA (noted HA-Rac-Ubn). An anti-HA immunoblot was performed in parallel on 1% of the total lysates to compare the amounts of total HA-Rac engaged in the His-Ub purifications (bottom).
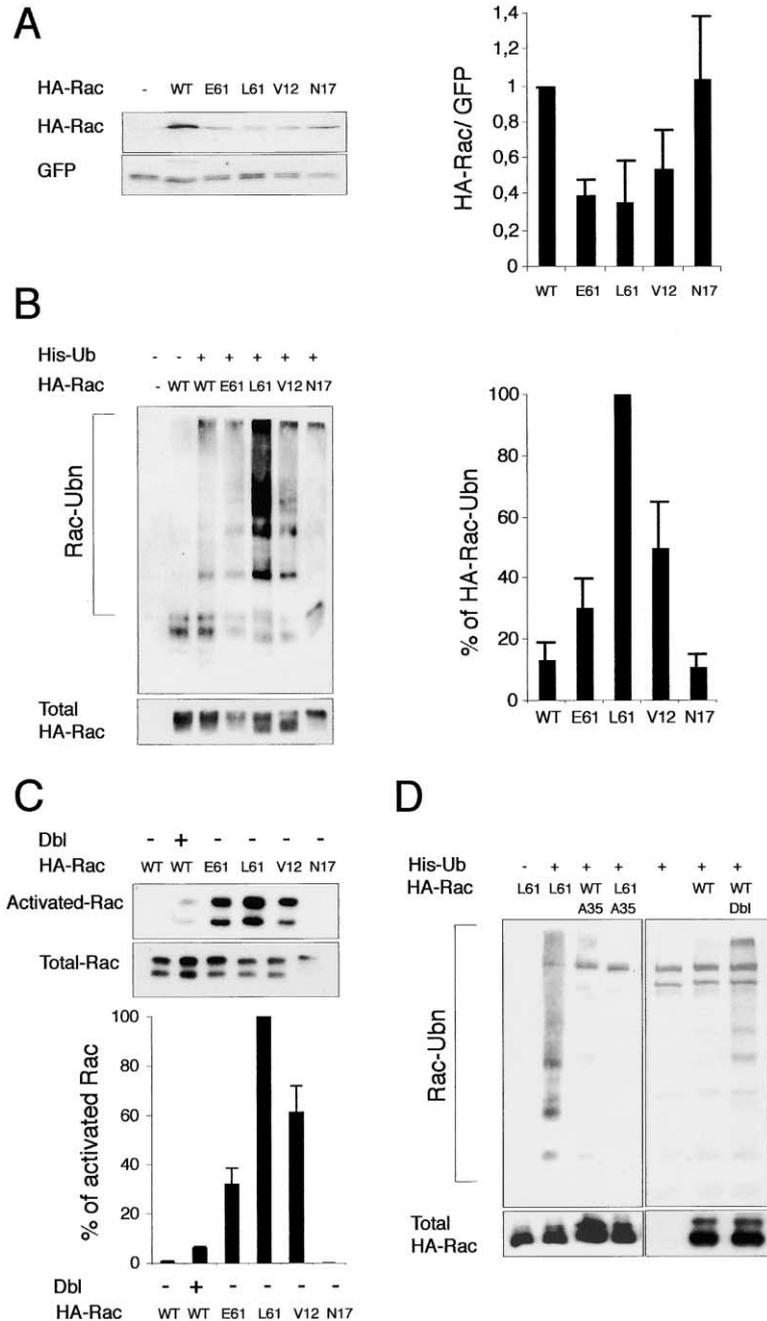
Figure 4. Activated Rac Mutants Are Highly Sensitive to Ubiquitylation

(A) Stability of Rac mutants in 804G cells. Cells were cotransfected with both 1 μg of GFP and 2 μg of HA-Rac mutants expressing plasmids. Equal amounts of total lysates were resolved on 12% SDS-PAGE and immunoblotted with anti-HA and anti-GFP. Side graph: Quantification of Rac mutants stability was assessed by calculating the ratio between HA-Rac mutant protein levels and the respective GFP protein levels. A factor 1 stability was arbitrarily set for wild-type Rac (mean value of three independent experiments ± SD).

(B) His-Ub purification followed by anti-HA immunoblotting showing the Rac mutants ubiquitylation level in 804G cells. Transfected cells expressing His-tagged ubiquitin together with dominant-active forms of Rac mutants (HA-Rac-Q61E, -Q61L, or -G12V), wild-type (WT), or a dominant-inactive form (HA-Rac-T17N) were purified for histidine-tagged ubiquitylated-Rac and processed for HA-Rac immunoblotting. The HA-immunoblot in the lower gel shows the levels of transfected HA-Rac used. Side graph: Quantification of Rac mutant ubiquitylation efficiencies corresponding to the ratio of polyubiquitylated Rac (Rac-Ubn) to total Rac (mean value of three independent experiments ± SD).

(C) Measure of Rac activation. HA-Rac wild-type and mutants were expressed for 12 hr in 804G cells, together with Dbl$^{495-826}$ (referred to as Dbl) when indicated. Rac activation was assessed by pull-down assay. The graph shows the quantification of the activated Rac levels. A 100% value was arbitrarily set for Rac-Q61L (mean value of three independent experiments ± SD).

(D) Comparison of the ubiquitylation efficiencies between HA-Rac-Q61L, HA-Rac-T35A, HA-Rac-Q61L-T35A, and wild-type HA-Rac (±Dbl$^{495-826}$), as described in (B).

three dominant-positive forms of Rac appeared more susceptible to ubiquitylation with regard to both dominant-negative and wild-type Rac (Figure 4B). Rac mutant ubiquitylation sensitivity appeared to be a function of the strength of their respective activating mutation (Figure 4C). Specificity of activated Rac ubiquitylation was further investigated by mutating the threonine 35 of Rac, a mutation that was shown to impair the Ras switch transition required for effectors binding (Spoerner et al., 2001). As predicted from the above observations, mutation of threonine 35 reversed the ubiquitylation sensitivity of Rac-Q61 (Figure 4D). Finally, we measured that the sustained activation of Rac, using Dbl$^{495-826}$ exchange factor (Olson et al., 1996), resulted in a reproducible

2-fold increased sensitivity of Rac ubiquitylation (Figure 4C). The low level of Dbl-induced Rac ubiquitylation perfectly correlated with the limited stimulation potency of Dbl, as compared to activating mutations of Rac (Figure 4D). Studying CNF1, we could unravel that sustained activation of Rac sensitizes it to ubiquitylation. This prompted us to investigate whether CNF1 had exploited this downregulation of Rac to confer virulence properties to pathogenic bacteria.
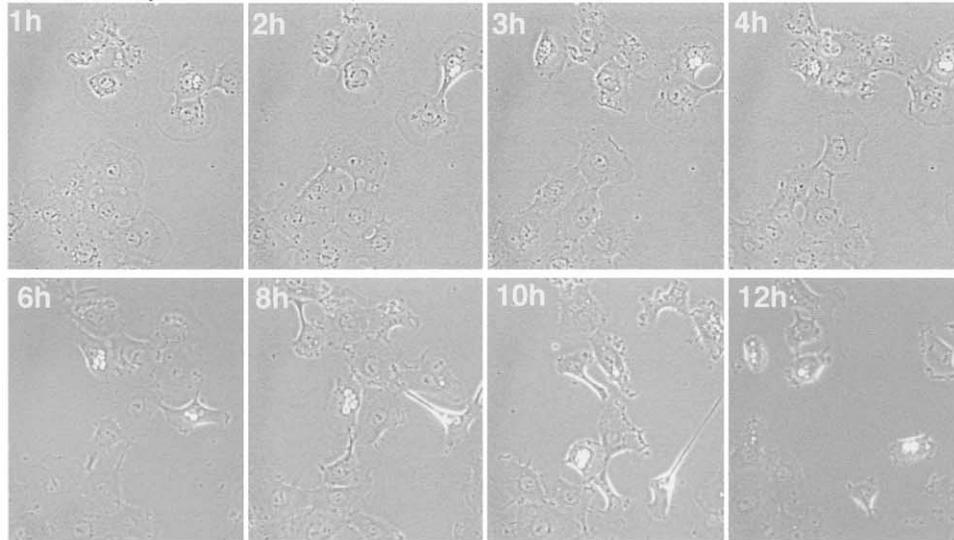
Proteasome Depletion of CNF1-Activated Rho GTPases Induces Cell Motility

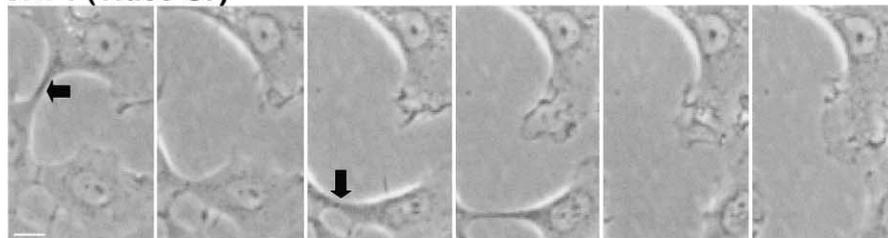We further analyzed the toxin-induced cellular morphological changes by time-lapse videomicroscopy during

A CNF1 (Video S1: 0-60 min.)
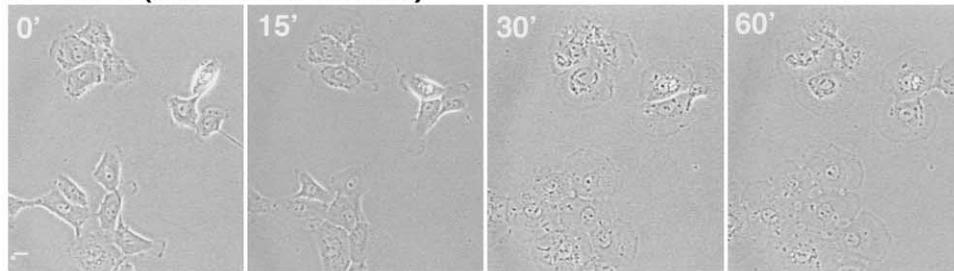
B CNF1 (Video S3: 1-6 h; Video S4: 6-12 h)

C CNF1 (Video S7)

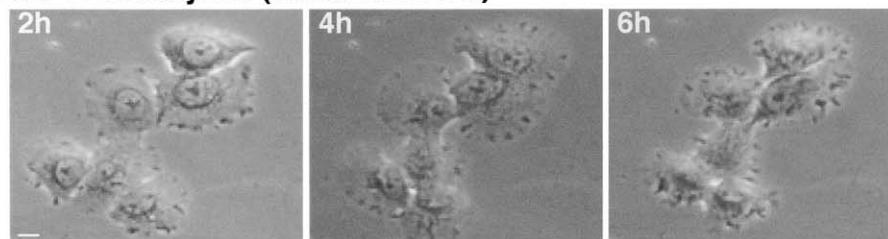## D CNF1+ lactacystin (Video S8: 2-6 h)

Figure 5. CNF1 Induces Cell Motility

(A) Visualization at four different timings of 804G cells intoxicated by 10^{-9} M CNF1, selected from Supplemental Video S1 at http://www.cell.com/cgi/content/full/111/4/553/DC1. This video documents the cell spreading during the first 60 min of intoxication (recorded at 1 frame/30 s and played at 1 frame per 1/30 s).

(B) Visualization of 10^{-9} M CNF1-intoxicated cells at eight different timings selected from Supplemental Videos S3 and S4 (recorded at 1 frame/30 s, using a 20× lens and played at 1 frame per 1/30 s). Supplemental Videos S3 and S4 document the sustained cell spreading during the first 4 hr, followed by the CNF1-induced cell motility. Supplemental Videos S1, S3, and S4 were recorded on the same field, using a 20× lens.

(C) Sequence of pictures, selected from Supplemental Video S7, showing the disruption of cellular junctions induced upon 6 hr of cells intoxication by 10^{-9} M CNF1 (recorded at 1 frame/60 s using a 40× lens and played at 1 frame per 1/30 s).

(D) Addition of proteasome inhibitor results in a blocking effect on the CNF1-induced cellular junctions dynamic and cell motility. Pictures depict three times selected from Supplemental Video S8. This video was recorded during 4 hr of cell intoxication starting after 2 hr addition of 10^{-9} M CNF1 and 20 μM lactacystin (recorded at 1 frame/60 s, using a 40× lens and played at 1 frame per 1/30 s). The bars equal 10 μm.

A

| CNF1 | - | - | - | - | 0 | 2 | 4 | 8 | 0 | 2 | 4 | 8 h |
| Cyclo | 0 | 2 | 4 | 8 | - | - | - | - | 0 | 2 | 4 | 8 h |

Actin

HA-Rac

B

CNF1 (Video S9: 3-9 h)

GFP + Rac   3h   8h   9h
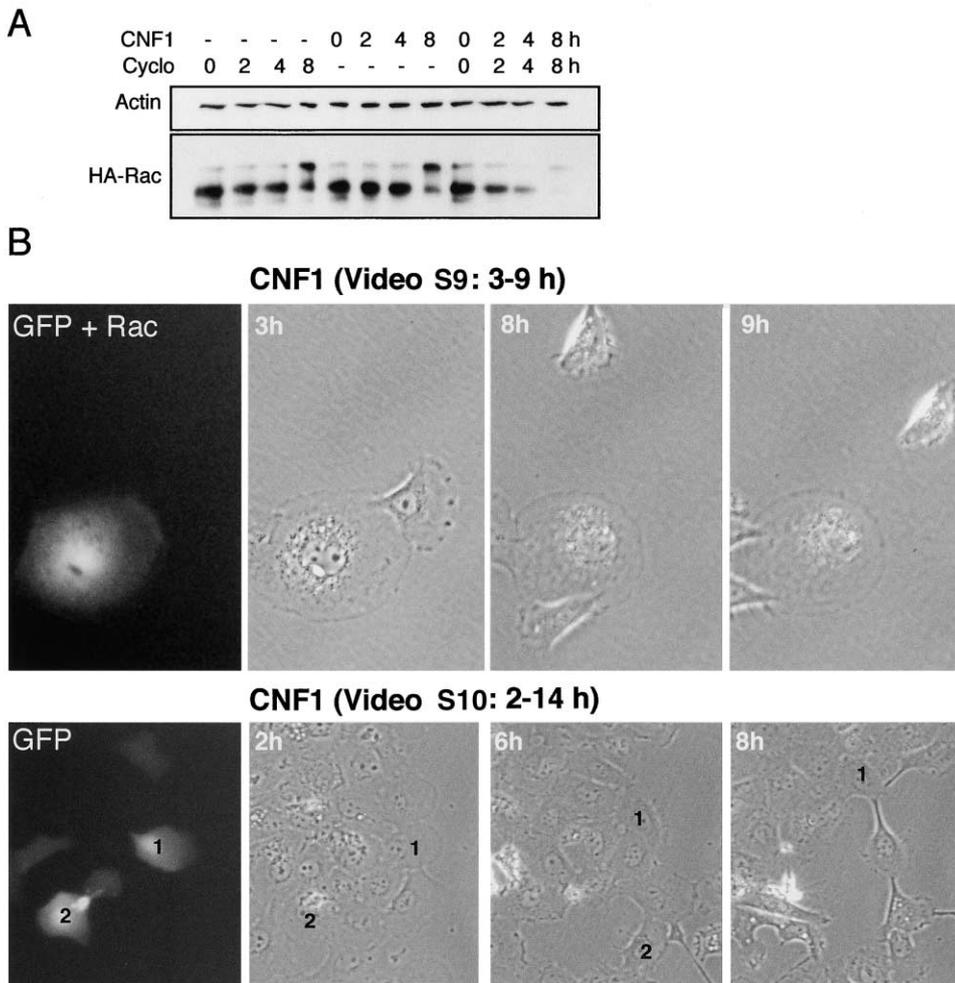
CNF1 (Video S10: 2-14 h)

GFP   2h   6h   8h

Figure 6. Overexpression of Rac Blocks CNF1-Induced Cell Motility

(A) Immunoblot anti-Rac1 showing the persistence of the HA-Rac signal in wild-type HA-Rac expressing 804G cells treated for different time periods with 10^{-9} M CNF1 alone or in combination with cycloheximide.

(B) Wild-type Rac overexpression inhibits the toxin-induced cell motility. Pictures were selected from Supplemental Videos S9 (GFP + Rac) and S10 (GFP alone). Supplemental Video S9 was performed from 3 to 9 hr after addition of 10^{-9} M CNF1 to 804G cells coexpressing wild-type Rac and GFP. Supplemental Video S10 was performed from 2 to 14 hr after addition of 10^{-9} M CNF1 to 804G cells expressing GFP alone. Both videos were recorded at 1 frame/30 s, using a 20× lens and played at 1 frame per 1/30 s.

the period corresponding to the previously measured kinetics of Rho GTPases activation and deactivation (Figure 1A). Figure 5 presents samples of pictures selected from the different videos. During the first hour of intoxication, corresponding to the Rho GTPases activation phase, cells underwent a strong spreading (Figure 5A and see Supplemental Video S1 at http://www.cell.com/cgi/content/full/111/4/553/DC1). We verified that heat-inactivated CNF1 did not induce such a cell phenotype (Supplemental Video S2). Spreading was followed by a period of intense membrane ruffling, from 1 to 4 hr, corresponding to the maximum activation of the Rho GTPases (Figure 5B and Supplemental Video S3). At 4 hr of intoxication, while proteasome activity started to reduce the level of activated Rho GTPases, membrane lamellipodia were progressively replaced by filopodia-like structures (Figure 5B and Supplemental Video S3). This process was accompanied by the induction of frank cell motility, 6 hr after intoxication up to 24 hr (Figure

5B and Supplemental Video S4). Moving cells displayed a classical pattern of polarity (Ridley, 2001), although cells migrated in random patterns, frequently changing their direction (Supplemental Video S4). In addition, we observed in primary HUVEC endothelial cells, a cellular model for K1 *E. coli* producing CNF1, a toxin-induced cellular motility starting 6 hr after intoxication and requiring the functional deamidase domain of the toxin (see Supplemental Videos S5 and S6, respectively). Following 804G cells spreading, during the raising of cell motility, we observed that cellular contacts were highly dynamic, constantly forming and dislocating (Figure 5C and Supplemental Video S7). Together, our observations pointed out the role of the proteasomal machinery in controlling the level of CNF1-induced Rho GTPase activation, resulting in cell motility during Rho GTPase depletion. Consistent with this, we observed that co-treatment with lactacystin during cell intoxication resulted in a sustained cell spreading and had a blocking
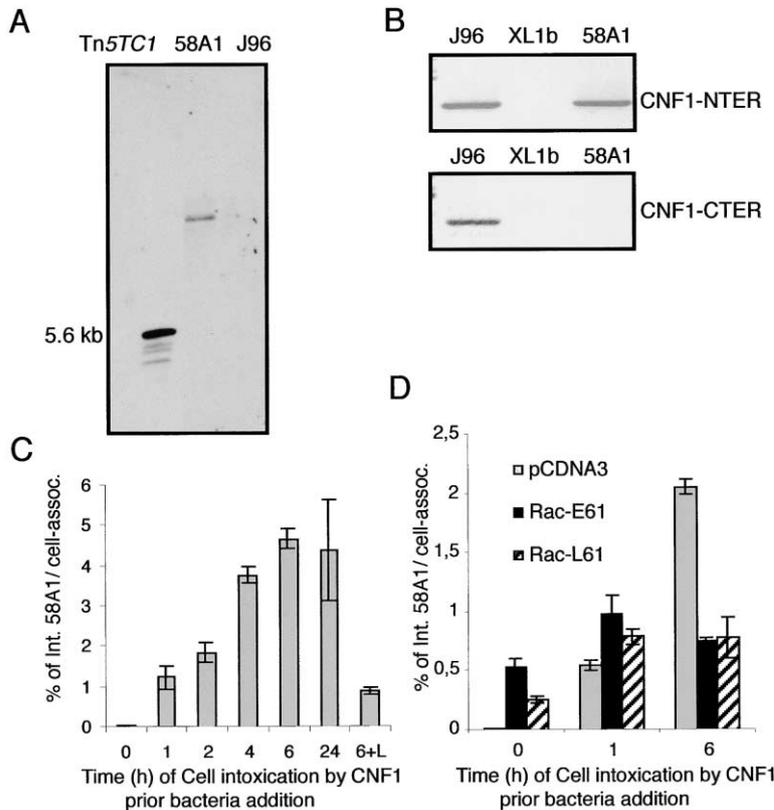
Figure 7. CNF1-Induced Uropathogenic Bacteria Internalization

(A) Southern blotting showing the presence or absence of Tn5 either in pBR322-Tn5TC1 plasmid or 58A1 conjugated and parental J96 genomic DNA. Genomic DNA was digested with BamH1 (outside Tn5) and probed with a Tn5TC1 0.6 kb EcoR1-Xba1 fragment, as described in the Experimental Procedures.
(B) DNA ethidium bromide staining of PCR amplification products of both cnf1-cter and -nter domain coding sequences performed on J96, 58A1, and XL1-blue genomic DNA.
(C) CNF1-induced 58A1 cell internalization. Monolayers treated for different times with 10^{-9} M CNF1, alone or with lactacystin when indicated (6+L), were proceeded for bacterial infection followed by gentamicin protection assay, as described in the Experimental Procedures. Values on the y axis represent the relative percent of intracellular bacteria, as compared to cell-associated bacteria (mean value of three independent experiments performed in duplicate ± SD).
(D) CNF1-induced 58A1 cell internalization in 804G cells expressing permanently activated Rac mutants. Values on the y axis represent the relative percent of intracellular bacteria, as compared to cell-associated bacteria (mean value of three independent experiments performed in duplicate ± SD).

effect on both cellular junction dynamics and cell motility (Figure 5D and Supplemental Video S8). The requirement of Rac degradation in allowing cell motility was further investigated, compensating for its degradation by wild-type Rac overexpression (Figure 6A). As hypothesized from the blocking effect of lactacystin, forced expression of Rac impaired the toxin-induced cell motility (Figure 6B and Supplemental Videos S9 and S10).

CNF1 producing gram-negative bacteria live in close contact with epithelial cell layers. This led us to investigate the effect of CNF1 on uroepithelial cell monolayers. Addition of CNF1 induced a sequence of cell-shape reorganization, similar to that of isolated cells and resulting in the raising of cell motility inside the monolayer (see Supplemental Video S11 at http://www.cell.com/cgi/content/full/111/4/553/DC1). Moreover, we observed that the cell motility inside the monolayer remained intense after a long period of intoxication, some cells seeping underneath each other (Supplemental Video S12). We also verified that heat-inactivated CNF1 did not induce cell movements (Supplemental Video S13). Together, our observations demonstrate that CNF1 provoked cell motility and cellular junction dynamics upon reduction of the activated Rac GTPase cellular level.

Rho GTPase Activation and Degradation Allow Efficient Host Cell Invasion

We further tested the implication of both CNF1-induced Rho GTPase activation and degradation phases for bacteria internalization into host cells. We generated a uropathogenic J96 bacteria (Low et al., 1984; Blum et al., 1995) knocked in cnf1, referred as 58A1 (Figures 7A and

7B). We verified the requirement of CNF1 for uropathogenic bacteria cell invasion, as previously described for K1 *E. coli* (Khan et al., 2002; see Supplemental Figure S1 at http://www.cell.com/cgi/content/full/111/4/553/DC1). Comparison of Rho GTPase activation and degradation phases in allowing bacterial invasion was tested by intoxication of 804G cells for different times prior to addition of 58A1 bacteria. Addition of CNF1 to cells appeared to be strictly required to allow bacteria internalization by nonphagocytic uroepithelial cells (Figure 7C). Interestingly, the efficiency of bacteria internalization started to increase during the Rho GTPase deactivation phase (around 4 hr of intoxication) (Figure 7C). That bacteria maximal internalization required both Rho GTPase activation and degradation (i.e., Rho GTPases restricted activation) was also supported by the observation that at 24 hr CNF1 intoxication, cells remained highly competent for bacteria internalization. In agreement with the fact that activated Rho GTPase degradation was required for efficient bacterial invasion, addition of lactacystin (which does not interfere with bacteria growth and viability) considerably reduced cell invasion (Figure 7C). Implication of Rho GTPase degradation was further demonstrated using 804G cells expressing permanently activated Rac mutants (Figure 7D). With regard to pcDNA3-transfected cells, we observed that activated Rac mutants expression reduced bacteria internalization to the low level induced by mere Rac activation observed at 1 hr (Figure 7D). Together, our results demonstrate that activation of Rac by CNF1 is required for initiating uropathogenic bacteria internalization by nonphagocytic uroepithelial cells and that Rac degrada-

tion, resulting in lowering the threshold of its activity, confers higher bacterial invasive characteristics to intoxicated cells.

Discussion

Using a bladder epithelial cell target model for CNF1, we could demonstrate that the bacterial toxin mechanism of action consists in a restricted stimulation of Rho GTPases. This CNF1-induced restricted activation is a direct consequence of the cell-mediated degradation of the toxin-activated forms of Rho GTPases. Degradation requires the proteasome machinery. More generally, we could demonstrate that the sustained activation of Rac resulted in its sensitization to ubiquitylation and proteasome degradation. Restricted activation of Rac by the dual CNF1 molecular mechanism appeared to be required for the toxin-induced cellular motility and UPEC efficient internalization by bladder epithelial cells. Our results thus provide evidence that CNF1 might be a bona fide invasive factor that exploits the host proteasomal machinery.

Since the discovery that CNF1 induces a posttranslational modification of Rho GTPases, resulting in their in vitro permanent activation, it was assumed that such a modification provoked the sustained activation of Rho GTPases in host cells (Flatau et al., 1997; Schmidt et al., 1997). We provide in fact new evidence that host cell intoxication by CNF1 only induces a transient activation of Rho GTPases, giving a maximal level of activated Rac and Cdc42. We have demonstrated that Rac is normally a stable protein and that, upon modification by CNF1, Rac is ubiquitylated and degraded. Consistent with this, we observed that inhibition of the proteasomal machinery allowed the recovery of higher levels of activated Rac. Our results indicate that depletion of Rho GTPases by the proteasome resulted from the higher kinetics of their deamidation and degradation not compensated by Rho GTPase synthesis.

The toxin-induced sensitivity of Rac to ubiquitylation and degradation could be generalized to other forms of permanently activated Rac. We first observed that Rac ubiquitylation efficiency correlated with the strength of the activating mutation, Q61L being the most sensitive one. Second, we observed that the T35A mutation, located in the effector binding domain, reversed the ubiquitylation sensitivity of Rac-Q61L. Finally, our observation that a sustained activation of Rac, using Dbl, also sensitized Rac to ubiquitylation proportional to its activation level eliminated a possible degradation of Rac due to mere protein misfolding. Depletion of Rho GTPases by CNF1 required several hours. This mechanism obviously cannot be used by cells to rapidly downregulate a stimulation of Rho GTPases, for instance by growth factors, and therefore does not substitute for Rho GTPase activating proteins (GAP). One possibility would be that this mechanism constitutes a vigilance system elaborated by cells to counteract the nocuous effects of a permanent activation of Rho GTPases for cell homeostasy. Consistent with this, we observed a lower CNF1-induced degradation rate of Rac in some carcinoma cells. This correlated to a 10-fold lower capacity of Rac ubiquitylation, for instance in HEp-2 larynx carcinoma cells, as compared to the ubiquitylation rate

of Rac measured in primary endothelial HUVEC or in 804G cells (see Supplemental Figure S2 at http://www.cell.com/cgi/content/full/111/4/553/DC1). Another nonexclusive possibility would be that this mechanism might contribute to Rnd proteins regulation, a family of GTPase-deficient Rho-like proteins (Nobes et al., 1998; Li et al., 2002).

Concurrent with the proteasome-dependent reduction of the activated Rho GTPases cellular levels, intoxicated cells started to produce membrane extensions and retractions associated with cell movement and cellular connection remodeling. Restricted activation of Rho GTPases by the toxin appeared to be sufficient to control the basic machinery necessary for cell movements. Consistent with our model, we could block the CNF1-induced cell motility either by addition of lactacystin or Rac sustained expression. We could also observe that in contrast to 804G cells and HUVEC cells, sustained activation of Rac in HEp-2 cells resulted in a lack of cell motility (see Supplemental Video S14 at http://www.cell.com/cgi/content/full/111/4/553/DC1). Our observations raised the question of whether CNF1-induced cell motility might contribute to bacteria colonization and/or epithelium invasion. One hypothesis could be that upon attachment of the bacteria to the host cells, induction of cell streaming by the toxin might contribute to bacterial spreading at the surface of the epithelium, thereby favoring the colonization of new territories. In addition to cell migration, cellular contact remodeling might contribute to pathogenic bacteria invasion of deeper parts of the epithelium.

The idea that degradation of Rho GTPases upon their activation does not represent a host response to a pathogen attack, but rather a response exploited by the pathogen, is strengthened by our observation that permanently activated Rac degradation allows not only host cell motility but also confers higher invasive properties to bacteria. These two features may contribute to the success of bacterial epithelium invasion, which is important for urinary tract infection (Mulvey et al., 2000). Interestingly, the pathogenic bacteria *Salmonella* delivers antagonistic Rho GTPase regulatory molecules, namely SopE and SptP. The SopE exchange factor activity toward Rac and Cdc42 is responsible for their activation, whereas the SptP GAP activity provokes their inactivation, leading to the notion of a pathogen self-restricted response (Galàn and Zhou, 2000). UPEC expressing CNF1 may have thus developed a system for mimicking a GEF/GAP Rho GTPase limited activation, resulting in host cell invasion and motility.

Pathogenic bacteria-induced host cell internalization is a hallmark of invasion and sepsis. In view of the CNF1 mechanism of action, further work should elucidate both CNF1 implication in *E. coli*-induced meningitis and recurrent cystitis. We provide definitive evidence that efficient bacteria invasion is realized by limiting the threshold of Rac activation and that CNF1 has achieved this condition by exploiting the ability of cells to withdraw permanently activated Rho GTPases.

Experimental Procedures

Transfection, Materials, and Constructs
804G rat bladder carcinoma cells were propagated in DMEM 10% fetal bovine serum (GIBCO-BRL, Paisley, Scotland). Transfections

were performed by electroporation, except for pEGFP-C2-CDD constructs, which were transfected using ExGen 500 (Euromedex, France) with 2 μg of plasmid. Electroporations were performed as follows: 5 $\times$ 10[6] cells were electroporated with 30 μg of total DNA at 300V, 450 μF. The efficiency was approximately 30% using both methods, as assessed by epifluorescence microscopy of cells transfected with pEGFP-C2 (Clontech, Palo-Alto, CA). When indicated, cells were treated with the following inhibitors: Z-VAD, MG132, ALLN (referred as LLnL), and Lactacystin (Calbiochem, CA).

Rac mutants were obtained using the QuickChange Site Directed Mutagenesis Kit (Stratagene Europe, The Netherlands) on pXJ-HA-Rac wild-type (Manser et al., 1998), containing the polymorphism I135T. HA-Rac mutants were obtained as follows: GAA for HA-Rac-Q61E, CTA for HA-Rac-Q61L, GTA for HA-Rac-G12V, GCC for HA-Rac-T35A, and AAC for HA-Rac-T17N. The absence of other mutations was verified by sequencing the entire coding region. GFP-CDD constructs were obtained by PCR amplification of the CNF1 sequence encompassing amino acids 720–1014. The PCR fragment was subcloned BamH1-EcoR1 in pEGFP-C2 (Clontech). GFP-CDD$_{C866A}$ was obtained by QuickChange Site Directed Mutagenesis, converting the coding sequence of cysteine 866 into GCT.

CNF1 and CNF1$_{C866S}$ toxins were purified as described previously (Flatau et al., 1997).

Antibodies were purchased from Transduction Laboratories (anti-Rac1, anti-Rho [raised against a sequence of RhoA highly homologous to RhoB and RhoC], anti-Cdc42, anti-RalA, anti-Rap1, and anti-Ras), from Santa Cruz (anti-RhoGDI [clone A-20]), from BabCo (anti-HA [clone 11]), from Sigma (St. Louis, MO) (anti-β actin [clone AC-74]), and from Roche (Mannheim, Germany) (anti-GFP [clones 7.1 and 13.1]). Primary antibodies were visualized using goat anti-mouse or anti-rabbit horseradish peroxidase-conjugated secondary antibodies (DAKO, Glostrup, Denmark) followed by chemiluminescence detection (ECL, Amersham, Buckinghamshire, UK).

Activated Rho GTPase Pull-Down

Pull-down assays were performed using 1 mg of cell lysate for Rho and Cdc42 or 0.5 mg for Rac, using 40 μg of either GST-PAK[70–106] for Rac and Cdc42 or GST-Rhotekin RBD for Rho, as described (Manser et al., 1998; Ren et al., 1999). Two percent of the control CNF1-untreated total lysate was loaded to estimate the Rho GTPases cellular content in order to quantify the ratio of CNF1-activated Rho GTPases. Proteins were resolved on 12% SDS-PAGE followed by transfer on PVDF membranes (Amersham, Saclay, France). Activated Rho GTPases were revealed by immunoblotting using monoclonal anti-Rho GTPases. In parallel, the equal amount of proteins engaged in the pull-down assays was confirmed by immunoblotting anti-β-actin.

Metal-Affinity Precipitation

For endogenous Rac ubiquitylation measurements, cells were transfected by electroporation either with pRBG4-6HisUb or pRBG4-6HisUbK48R (30 μg/5 $\times$ 10[6] cells). Three hours after transfection, cells were either untreated or treated 15 hr with 10^{−8} M CNF1, as indicated, and lysed in ULB (8 M Urea, 20 mM Tris-HCl [pH 7.5], 200 mM NaCl, 10 mM imidazole, and 0.1% Triton X-100). The quantities of Rac mutants present in the clarified lysates were first determined on immunoblots in order to use equal quantities of Rac mutants in the histidine-tag purifications. Normalized HA-Rac lysates were purified for histidine-tagged ubiquitin on 30 μl cobalt chelated resin (Clontech), previously incubated in 5% bovine serum albumin (RIA grade, Sigma). After lysate incubation, the beads were washed four times in ULB and once in PBS and resuspended in one volume of Laemmli buffer. Proteins were resolved on a 12% SDS-PAGE, and polyubiquitylated Rac was visualized by immunoblotting anti-HA. For other Rac ubiquitylation measurements, cells were transfected by electroporation with pRBG4-6HisUb (15 μg/5 $\times$ 10[6] cells) and pXJ-HA-Rac wild-type and mutants (15 μg/5 $\times$ 10[6] cells). For Dbl experiments, either pcDNA3 or pRK5-myc-Dbl[495-826] (5 μg/5 $\times$ 10[6] cells) were added to the mixture (Olson et al., 1996). The efficiency of Rac mutant ubiquitylation was assessed after 16 hr expression. Graphs correspond to the ratio of the Rac-Ubn signal to the total HA-Rac signal.

Immunofluorescence and Time Lapse Imaging

Cells were fixed in 4% paraformaldehyde (Sigma) and permeabilized with 0.05% saponin (Sigma). Rac immunolocalization was per-

formed using the anti-Rac1 antibody described above and was visualized using Texas red-conjugated anti-mouse mAb (Vector, Biovalley, Marne la Vallée, France). Actin cytoskeleton was labeled using 1 μg·ml^{−1} FITC-conjugated phalloidin (Sigma). Immunosignals were analyzed with a TCS-SP confocal microscope (Leica, Heidelberg, Germany) using a 63$\times$ magnification lens. Each picture represents the projection of eight serial confocal optical sections. In order to compare the Rac immunosignal intensities during the time course of CNF1 cell intoxication, we set up standard conditions of signal acquisition for this GTPase on the 1 hr CNF1-treated cell sample. We verified the absence of "bleed-through" for both signals. Cells were filmed for different periods of time, in constant conditions of 5% CO_2 and 37°C, and observed by phase-contrast optics using an Axiovert 200 microscope (Carl Zeiss, Göttingen, Germany) with shutter-controlled illumination (Carl Zeiss) and a cooled, digital CCD camera (Roper Scientific) using a 40$\times$ or 20$\times$ lens, as indicated. Images were recorded at 1 frame/30–60 s depending on the conditions and processed using MetaMorph 2.0 image analysis software (Universal Imaging) and QuickTime pro 5 software (Apple).

Construction of J96 Knocked-in cnf1 and 804G-Cell Monolayer Infection

The E. coli 58A1 strain, corresponding to J96 cnf1::Tn5, was obtained by standard conjugation of J96 with Bug 241 containing pBR322-Tn5TC1 (Sasakawa and Yoshikawa, 1987). Conjugated bacteria were screened for the absence of CNF1 expression using a multinucleation assay with HEp-2 cells (Lemichez et al., 1997). Four strains of conjugated bacteria were isolated out of 3500. 58A1 was found to have a unique insertion of Tn5 by Southern blotting of genomic DNA digested BamH1, using a 0.6 kb EcoR1-Xba1 Tn5TC1 probe and the dig high-prime DNA labeling and detection starter kit II (Roche). Tn5 insertion in the 58A1 cnf1 carboxy-terminal domain was assessed by PCR using the following primers (ATGGGTAAC CAATGGCAAC and GCGTTTCTTAACAGAAATAGC for NTER amplification and AGTATCGAAAGCACCTCCT and TCAAAATTTTTTTG AAAATACCTTC for CTER amplification). For bacterial infection assay, 4 $\times$ 10[5] uroepithelial cells were seeded per 35 mm well 24 hr before infection. 10:1 exponentially growing 58A1 bacteria were added to cell monolayers intoxicated with 10^{−9} M CNF1 for different periods of time supplemented with 20 μM lactacystin if indicated. Internalization was allowed during 15 min at 37°C after 5 min centrifugation at 1000 rpm. Infected monolayers were either washed three times and lysed for cell-associated bacteria measurement (about 5% of total bacteria) or washed once and incubated 20 min with 50 μg·ml^{−1} gentamicin before lysis for internalized bacteria measurements (Falkow et al., 1987). Cells were lysed in PBS, 0.1% triton X-100 and bacteria were counted on LB ampicillin 100 μg·ml^{−1} plates. When indicated, 804G cells were transfected the day before by electroporation. The transfection efficiency based on Rac phenotype was about 50%.

References

Blanco, J., Blanco, M., Alonso, M.P., Blanco, J.E., Gonzalez, E.A., and Garabal, J.I. (1992). Characteristics of haemolytic Escherichia coli with particular reference to production of cytotoxic necrotizing factor type 1 (CNF1). Res. Microbiol. 143, 869–878.

Blum, G., Falbo, V., Caprioli, A., and Hacker, J. (1995). Gene clusters encoding the cytotoxic necrotizing factor type 1, Prs-fimbriae and

alpha-hemolysin form the pathogenicity island II of the uropatho-genic *Escherichia coli* strain J96. FEMS Microbiol. Lett. *126*, 189–195.

Bonacorsi, S.P., Clermont, O., Tinsley, C., Le Gall, I., Beaudoin, J.C., Elion, J., Nassif, X., and Bingen, E. (2000). Identification of regions of the *Escherichia coli* chromosome specific for neonatal meningitis-associated strains. Infect. Immun. *68*, 2096–2101.

Boquet, P. (2001). The cytotoxic necrotizing factor 1 (CNF1) from *Escherichia coli*. Toxicon *39*, 1673–1680.

Boquet, P., Munro, P., Fiorentini, C., and Just, I. (1998). Toxins from anaerobic bacteria: specificity and molecular mechanisms of action. Curr. Opin. Microbiol. *1*, 66–74.

Buetow, L., Flatau, G., Chiu, K., Boquet, P., and Ghosh, P. (2001). Structure of the Rho-activating domain of *Escherichia coli* cytotoxic necrotizing factor 1. Nat. Struct. Biol. *8*, 584–588.

Chardin, P., Boquet, P., Madaule, P., Popoff, M.R., Rubin, E.J., and Gill, D.M. (1989). The mammalian G protein rhoC is ADP-ribosylated by *Clostridium botulinum* exoenzyme C3 and affects actin microfila-ments in Vero cells. EMBO J. *8*, 1087–1092.

Chau, V., Tobias, J.W., Bachmair, A., Marriott, D., Ecker, D.J., Gonda, D.K., and Varshavsky, A. (1989). A multiubiquitin chain is confined to specific lysine in a targeted short-lived protein. Science *243*, 1576–1583.

Falkow, S., Small, P., Isberg, R., Hayes, S.F., and Corwin, D. (1987). A molecular strategy for the study of bacterial invasion. Rev. Infect. Dis. *9*, 450–455.

Flatau, G., Lemichez, E., Gauthier, M., Chardin, P., Paris, S., Fioren-tini, C., and Boquet, P. (1997). Toxin-induced activation of the G protein p21 Rho by deamidation of glutamine. Nature *387*, 729–733.

Flatau, G., Landraud, L., Boquet, P., Bruzzone, M., and Munro, P. (2000). Deamidation of RhoA glutamine 63 by the *Escherichia coli* CNF1 toxin requires a short sequence of the GTPase switch 2 do-main. Biochem. Biophys. Res. Commun. *267*, 588–592.

Galàn, J.E., and Zhou, D. (2000). Striking a balance: modulation of the actin cytoskeleton by *Salmonella*. Proc. Natl. Acad. Sci. USA *97*, 8754–8761.

Hall, A. (1998). Rho GTPases and the actin cytoskeleton. Science *279*, 509–514.

Hershko, A., and Ciechanover, A. (1998). The ubiquitin system. Annu. Rev. Biochem. *67*, 425–479.

Horiguchi, Y. (2001). *Escherichia coli* cytotoxic necrotizing factors and *Bordetella dermonecrotic* toxin: the dermonecrosis-inducing toxins activating Rho small GTPases. Toxicon *39*, 1619–1627.

Khan, N.A., Wang, Y., Kim, K.J., Chung, J.W., Wass, C.A., and Kim, K.S. (2002). Cytotoxic necrotizing factor-1 contributes to *Escherichia coli* K1 invasion of the central nervous system. J. Biol. Chem. *277*, 15607–15612.

Landraud, L., Gauthier, M., Fosse, T., and Boquet, P. (2000). Fre-quency of *Escherichia coli* strains producing the cytotoxic necrotiz-ing factor (CNF1) in nosocomial urinary tract infections. Lett. Appl. Microbiol. *30*, 213–216.

Lemichez, E., Flatau, G., Bruzzone, M., Boquet, P., and Gauthier, M. (1997). Molecular localization of the *Escherichia coli* cytotoxic necrotizing factor CNF1 cell-binding and catalytic domains. Mol. Microbiol. *24*, 1061–1070.

Lerm, M., Selzer, J., Hoffmeyer, A., Rapp, U.R., Aktories, K., and Schmidt, G. (1999a). Deamidation of Cdc42 and Rac by *Escherichia coli* cytotoxic necrotizing factor 1: activation of c-Jun N-terminal kinase in HeLa cells. Infect. Immun. *67*, 496–503.

Lerm, M., Schmidt, G., Goehring, U.M., Schirmer, J., and Aktories, K. (1999b). Identification of the region of rho involved in substrate recognition by *Escherichia coli* cytotoxic necrotizing factor 1 (CNF1). J. Biol. Chem. *274*, 28999–29004.

Li, X., Bu, X., Lu, B., Avraham, H., Flavell, R.A., and Lim, B. (2002). The hematopoiesis-specific GTP-binding protein RhoH is GTPase deficient and modulates activities of other Rho GTPases by an inhib-itory function. Mol. Cell. Biol. *22*, 1158–1171.

Lockman, H.A., Gillespie, R.A., Baker, B.D., and Shakhnovich, E.

(2002). *Yersinia pseudotuberculosis* produces a cytotoxic necrotiz-ing factor. Infect. Immun. *70*, 2708–2714.

Low, D., David, V., Lark, D., Schoolnik, G., and Falkow, S. (1984). Gene clusters governing the production of hemolysin and mannose-resistant hemagglutination are closely linked in *Escherichia coli* serotype O4 and O6 isolates from urinary tract infections. Infect. Immun. *43*, 353–358.

Manser, E., Loo, T.H., Koh, C.G., Zhao, Z.S., Chen, X.Q., Tan, L., Tan, I., Leung, T., and Lim, L. (1998). PAK kinases are directly coupled to the PIX family of nucleotide exchange factors. Mol. Cell *1*, 183–192.

Mulvey, M.A., Schilling, J.D., Martinez, J.J., and Hultgren, S.J. (2000). Bad bugs and beleaguered bladders: interplay between uropatho-genic *Escherichia coli* and innate host defenses. Proc. Natl. Acad. Sci. USA *97*, 8829–8835.

Nobes, C.D., Lauritzen, I., Mattei, M.G., Paris, S., Hall, A., and Char-din, P. (1998). A new member of the Rho family, Rnd1, promotes disassembly of actin filament structures and loss of cell adhesion. J. Cell Biol. *141*, 187–197.

Olson, M.F., Pasteris, N.G., Gorski, J.L., and Hall, A. (1996). Facio-genital dysplasia protein (FGD1) and Vav, two related proteins re-quired for normal embryonic development, are upstream regulators of Rho GTPases. Curr. Biol. *6*, 1628–1633.

Paterson, H.F., Self, A.J., Garrett, M.D., Just, I., Aktories, K., and Hall, A. (1990). Microinjection of recombinant p21rho induces rapid changes in cell morphology. J. Cell Biol. *111*, 1001–1007.

Pei, S., Doye, A., and Boquet, P. (2001). Mutation of specific acidic residues of the CNF1 T domain into lysine alters cell membrane translocation of the toxin. Mol. Microbiol. *41*, 1237–1247.

Ren, X.D., Kiosses, W.B., and Schwartz, M.A. (1999). Regulation of the small GTP-binding protein Rho by cell adhesion and the cytoskeleton. EMBO J. *18*, 578–585.

Ridley, A. (2001). Rho GTPases and cell migration. J. Cell Sci. *114*, 2713–2722.

Sasakawa, C., and Yoshikawa, M. (1987). A series of Tn5 variants with various drug-resistance markers and suicide vector for transpo-son mutagenesis. Gene *56*, 283–288.

Schmidt, G., Sehr, P., Wilm, M., Selzer, J., Mann, M., and Aktories, K. (1997). Gln 63 of Rho is deamidated by *Escherichia coli* cytotoxic necrotizing factor-1. Nature *387*, 725–729.

Spoerner, M., Herrmann, C., Vetter, I.R., Kalbitzer, H.R., and Witting-hofer, A. (2001). Dynamic properties of the Ras switch I region and its importance for binding to effectors. Proc. Natl. Acad. Sci. USA *98*, 4944–4949.

Stebbins, C.E., and Galán, J.E. (2001). Structural mimicry in bacterial virulence. Nature *412*, 701–705.

Note Added in Proof

During the course of our manuscript revision, the observation that CNF1-induced depletion of Rac is blocked upon cell cotreatment with lactacystin has been described in HEK293 cells by Lerm, M., Pop, M., Fritz, G., Aktories, K., and Schmidt, G. (2002). Proteasomal degradation of cytotoxic necrotizing factor 1-activated rac. Infect. Immun. *70*, 4053–4058.